Key Engineering Materials
ISSN: 1662-9795, Vol. 1057, pp 13-17
doi:10.4028/p-0rgVLc

Submitted: 2025-09-05
Revised: 2026-01-21
Accepted: 2026-01-31
Online: 2026-05-21

Impact of Device Structure on the Performance of Ion-Implanted SiC Phototransistors

Yang Liu[1,a*], Lei Yuan[1,b*], Xuesong Liu[2,c], Tongxiao Hou[2,d], Bo Peng[1,e], Renxu Jia[1,f] and Yuming Zhang[1,g]

[1]Faculty of Integrated Circuit, Xidian University, Xi'an 710071, China

[2]Beijing BJAST Holdings Co., Ltd., Beijing, China

[a*]23111110095@stu.xidian.edu.cn, [b]yuanlei@xidian.edu.cn, [c]lxs6721@126.com, [d]644988605@qq.com, [e]boopeng@xidian.edu.cn, [f]rxjia@mail.xidian.edu.cn, [g]zhangym@xidian.edu.cn

Keywords: bipolar phototransistor, ultraviolet, far-UVC detection.

Abstract. The far-UVC band (200–240 nm) is highly attractive for germicidal and solar-blind detection. To address limited surface carrier collection in epitaxial SiC phototransistors, we designed fully ion-implanted lateral phototransistors by combining transistor physics with CMOS-compatible processing. The lateral base width was systematically varied from 1 to 8 μm to investigate its influence on carrier transport and gain. A narrower base significantly enhanced photocurrent amplification, with the 1 μm device reaching 100.7 A/W at 200 nm and 60.0 A/W at 240 nm, while maintaining amplification up to the ~380 nm cutoff. Moreover, dark currents remained as low as 10^{-11} A, confirming the advantage of structural engineering for high-performance far-UVC SiC phototransistors.

Introduction

Applications such as astronomical detection, biomedical imaging, and solar-blind communication demand highly efficient ultraviolet detectors operating in the Far-UVC band [1–3]. Silicon carbide (SiC), owing to its wide bandgap, inherently possesses wavelength selectivity for ultraviolet detection. Moreover, its low intrinsic carrier concentration enables photodetectors fabricated from this material to exhibit exceptionally low dark current levels. Beyond these advantages, high-performance UV detectors are also expected to demonstrate excellent responsivity, that is, the capability to amplify weak optical signals. In this respect, bipolar phototransistors (BPTs) and avalanche photodiodes (APDs) offer significant benefits over conventional photodiodes, metal–semiconductor–metal (MSM) detectors, and other similar device architectures. While APDs are particularly suited for ultra-high-sensitivity detection, phototransistors present advantages in terms of compatibility with integrated design and operation under low bias voltages.

SiC epitaxial technology is comparatively mature and cost-effective, making it a long-standing preferred choice for fabricating not only photodetectors but also power and compact electronic devices. Numerous research groups have successfully demonstrated SiC-based bipolar phototransistors employing multiple epitaxial growth steps. However, from the perspective of quantum efficiency, these devices still struggle to achieve effective optical signal amplification [4–6]. With the advancement of SiC device technology, ion implantation has been increasingly adopted in device fabrication, gradually narrowing the gap between ion-implanted photodetectors and their epitaxial counterparts [7].

In this work, we report for the first time the design and implementation of several ion-implanted phototransistor architectures realized through CMOS-compatible processes. We provide a comprehensive evaluation of their optoelectronic performance, including dark current density, responsivity, quantum efficiency, and detectivity, and further elucidate how device structure influences these parameters.

This class of detectors effectively overcomes the long-standing limitation of SiC phototransistors in achieving practical optical signal amplification, while simultaneously revealing a set of effective design guidelines for the structural optimization of SiC-based phototransistors.

Device Structure and Process Design Based on Phototransistor Operation

The operating principle of a bipolar phototransistor relies on the separation of photon-generated electron–hole pairs by the reverse-biased base–collector (BC) junction. Under the influence of the electric field, holes drift into the base region. The accumulation of holes raises the base potential at the base–emitter (BE) junction, driving it into forward bias. This, in turn, facilitates electron injection from the emitter into the base, thereby realizing bipolar amplification. Consequently, the BC junction must sustain a stable photocurrent to ensure effective forward biasing of the BE junction. Once the concentration of separated holes is insufficient to maintain this condition, the device can no longer operate in the amplification mode.

In epitaxially grown structures, this limitation is often observed due to the exponential attenuation of photons within semiconductors, with the penetration depth strongly dependent on wavelength. For materials such as silicon operating in the infrared regime, the photon penetration depth can extend to several hundred micrometers. Hence, in Si-based infrared detectors, strategies such as stacking multiple epitaxial layers and extending the space-charge region are commonly employed to maximize photon absorption and collection [8]. In contrast, the design logic for ultraviolet detection is fundamentally different. For instance, at a wavelength of 244 nm, the penetration depth in SiC is only about 0.7 μm [9]. As a result, when the depth of the epitaxially formed space-charge region approaches or falls below this value, only a negligible fraction of photons can reach the reverse-biased depletion region. The correspondingly scarce hole population generated in this case is insufficient to maintain forward amplification in the phototransistor.

However, phototransistor structures formed by ion implantation can effectively address this issue. In this case, photons can directly reach the surface depletion region without significant attenuation, thereby substantially increasing the photocurrent generated at the base–collector (BC) junction and making it easier for the phototransistor to enter the amplification regime. Although this concept holds clear advantages in principle, several process-related considerations require special attention.

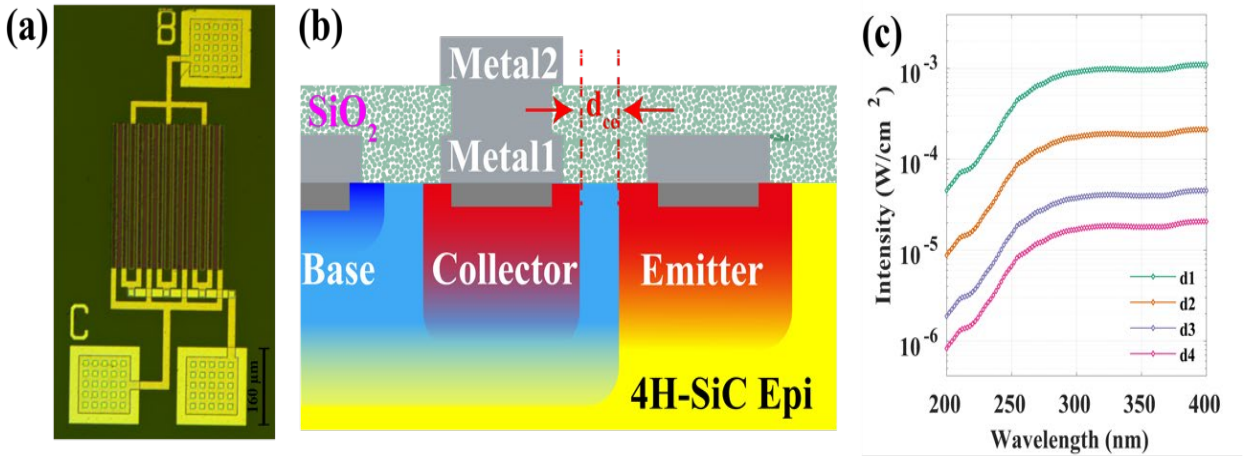

Fig. 1. (a) Top-view optical micrograph; (b) Schematic diagram of the device structure (half unit); (c) The relationship between incident optical power density and wavelength used during the testing process.

First, in a conventional ion-implanted BJT structure, the BC buried junction is typically located relatively deep inside the substrate. To mitigate this, we attempt to utilize the N-type region within the P-well as the collector, while designating the epitaxial layer as the emitter. Second, because the near-surface BC junction generates a large photocurrent, amplification must also be achieved through a surface BJT configuration. Consequently, the design focus shifts from realizing a vertically thin-base BJT via implantation energy to constructing a laterally narrow-base BJT. On this basis, we

fabricated four types of phototransistors with lateral base widths of 1, 2, 4, and 8 μm, respectively. Third, the surface oxide inevitably contains a certain amount of fixed charges, which may influence surface recombination and leakage current [10,11]. To minimize such effects, we employed the highest-quality oxide deposition process available to us, avoiding wet oxidation techniques that are prone to introducing large densities of interface charges. In summary, the actual device structure of our designed phototransistor is illustrated in Fig. 1.

Test Methods and the Impact of Lateral Base Width Variation on Device Performance

The electrical characteristics of the devices were measured using a Keysight B1500A semiconductor parameter analyzer. Optical excitation was provided by an EQ-77 white light source driven by a laser, with the output wavelength selected through a monochromator. The optical power incident on the device was controlled by adjusting the distance (d1–d4) between the optical fiber and the sample, as illustrated in Fig. 1c. The corresponding optical power density was calibrated using a commercial Si-based photodetector (Zolix OPE-B3-UV), which had been previously calibrated by the National Institute of Metrology, China, to ensure measurement accuracy.

The dark current characteristics and the comparison of dark current density are shown in Fig. 2. It can be observed that the four devices exhibit generally consistent trends, with slight variations in the absolute magnitude of the dark current. Specifically, when the applied bias is below 4 V, the dark current remains relatively low, but increases significantly once the bias exceeds this threshold. This behavior can be attributed to base punch-through: under reverse bias of the BC junction, the collector is a heavily doped region. As the applied bias increases, the depletion region extends deeply into the base and rapidly connects with the depletion region of the BE junction, resulting in a sharp increase in current. This phenomenon is a direct consequence of swapping the emitter and collector roles in the device design. Within the bias range below 4 V, the dark current densities of the four devices show minimal differences, all close to the measurement limit (10^{-10}–10^{-11} A). The slightly higher dark current in the device with a 1 μm lateral spacing is mainly attributed to the enhanced tunneling current caused by the abrupt doping gradient across the short distance [12], whereas increasing the spacing to 2 μm effectively suppresses this effect.

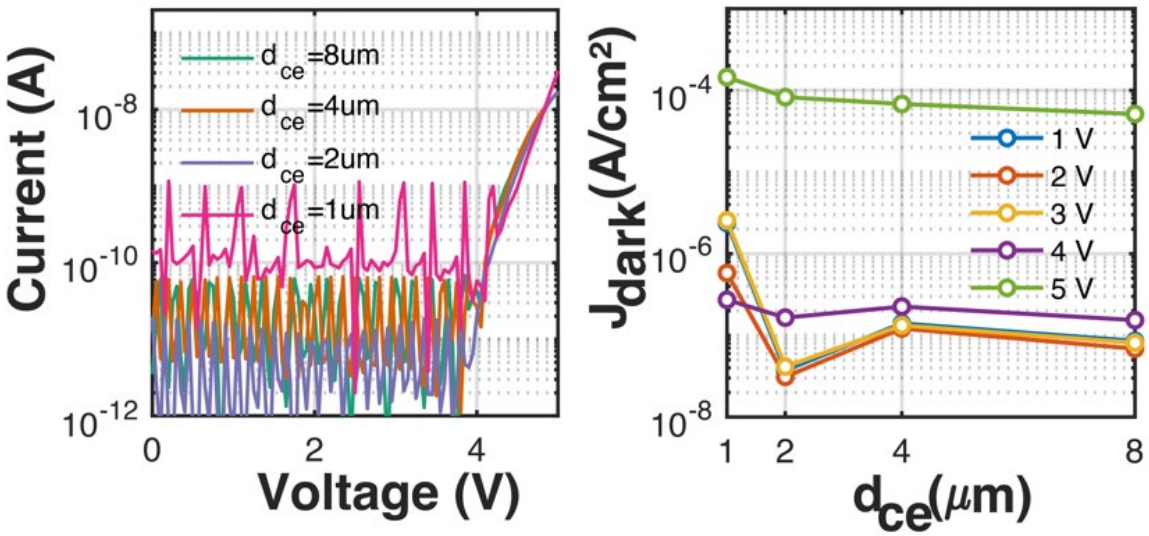

Fig. 2. Dark current characteristics for different CE spacings and bias.

The responsivity comparison and variation trends are illustrated in Fig. 3. First, under identical optical power density and excitation wavelength, the responsivity increases as the lateral base width decreases. In particular, devices with 2–8 μm base widths exhibit a significant reduction in responsivity compared to the 1 μm device. This can be explained by the fact that a narrower base width in the surface BJT enables more effective amplification. It can be anticipated that base widths

around 1 μm or even smaller could deliver stronger amplification; however, such scaling introduces a trade-off with the punch-through effect under operating bias, as discussed previously. Moreover, the difference in responsivity is more pronounced at 200 nm compared to 280 nm excitation (Fig. 3b and 3c).

Second, for the same device under identical wavelength excitation but varying optical power densities, it is clearly observed that responsivity increases as the optical power density decreases (d1 to d4). This result indicates that the near-surface BJT structure is more favorable for weak light detection.

Third, under constant optical power density but different excitation wavelengths, the responsivity at 200 nm is generally higher than at longer wavelengths. This suggests that the device is particularly well-suited for short-wavelength detection in the far-UVC region, as the shallower penetration depth of shorter-wavelength photons allows them to be more effectively absorbed and utilized by the surface BJT structure.

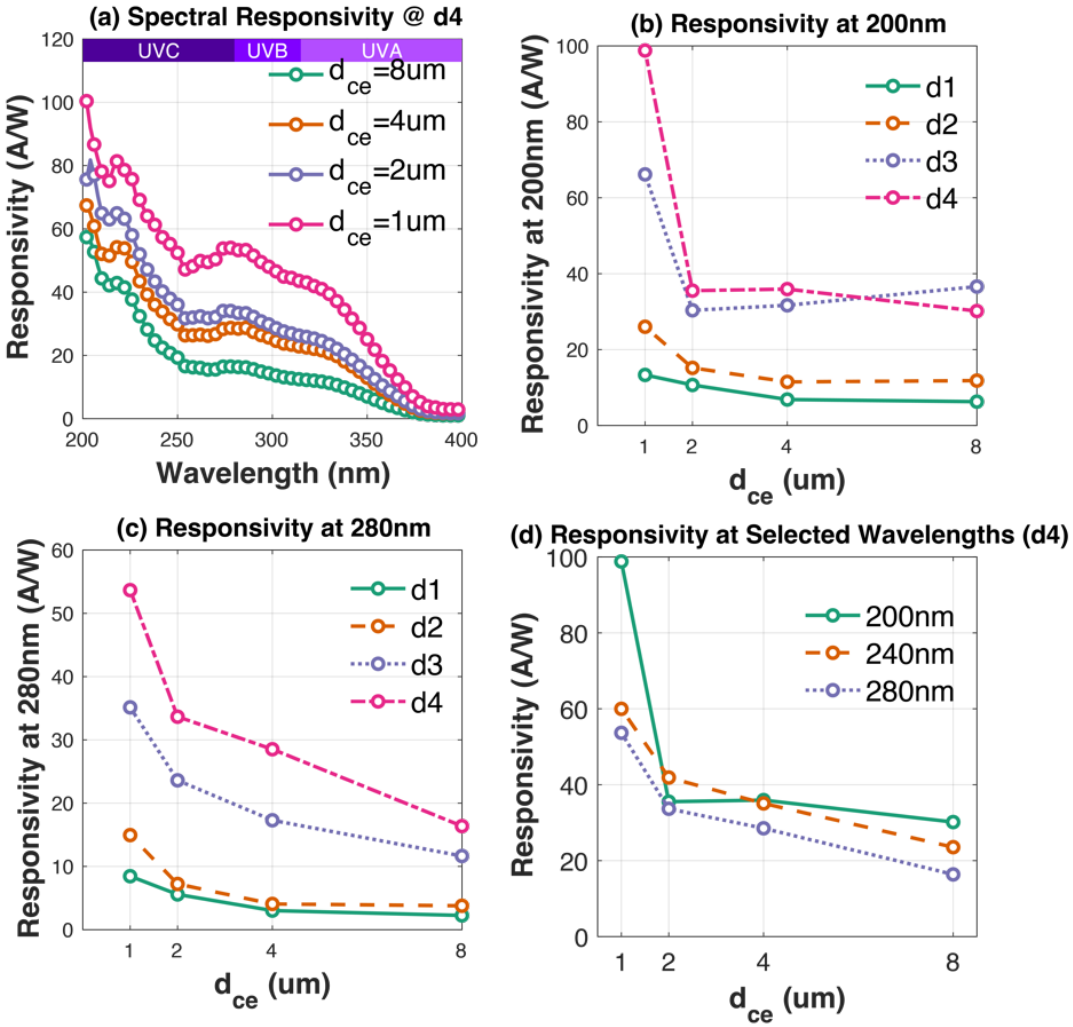

Fig. 3. (a) Spectral response under varying collector-emitter (CE) spacings. (b-d): Responsivity comparison of different UV light excitation.

Summary

The key performance metrics of the devices under 200 nm illumination are summarized in Table 1. It can be seen that under low-light conditions, the device with a collector–emitter spacing (d_{ce}) of 1 μm achieves a detectivity (D*) of 33.4×10^{13} Jones, whereas under high illumination intensities, the device with d_{ce} = 2 μm exhibits better detectivity. The responsivity of the 1 μm device reaches 100.7 A/W at 200 nm and 60.0 A/W at 240 nm, and photocurrent amplification is maintained across the entire spectral range up to the cutoff wavelength of approximately 380 nm.

Table I. Comparison of Key Parameters of Different PTs under 200 nm UV Illumination.

PT	J_{dark} (A/cm²)	R (A/W)		D* ($\times 10^{13}$ Jones)	
		d1	d4	d1	d4
d_{ce} = 8μm	1.53×10-7	6.29	30.16	2.8	13.5
d_{ce} = 4μm	2.25×10-7	6.85	35.94	2.5	13.3
d_{ce} = 2μm	1.64×10-7	10.68	35.53	**4.7**	15.4
d_{ce} = 1μm	2.72×10-7	13.33	**100.68**	4.5	**33.4**

These results collectively demonstrate that careful optimization of the device structure, particularly the lateral base width, plays a critical role in balancing responsivity, dark current, and detectivity in ion-implanted SiC phototransistors. Our study provides important insights for the future design of high-performance photodetectors targeting the far-UVC spectral region.

References

[1] Li, Jiaqi, Zhou, Yue, Yi, Xiangyu, et al., Current Optics and Photonics 1, 196–202 (2017).

[2] G. Wang, K. Wang, C. Gong, et al., IEEE Photonics J. 10, 1–13 (2018).

[3] D. Guo, Y. Su, H. Shi, et al., ACS Nano 12, 12827–12835 (2018).

[4] Y. Wang, W. Li, W. Xu, et al., IEEE Electron Device Lett. 45, 617–620 (2024).

[5] Y. Wang, W. Li, D. Zhou, et al., IEEE Trans. Electron Devices 1–8 (2022).

[6] C. Sun, H. Guo, L. Yuan, et al., IEEE Trans. Electron Devices 70, 2342–2346 (2023).

[7] C. D. Matthus, T. Erlbacher, A. J. Bauer, et al., "Comparative Study of 4H-SiC UV-Sensors with Ion Implanted and Epitaxially Grown p-Emitter," in 2018 22nd International Conference on Ion Implantation Technology (IIT) (IEEE, 2018), pp. 110–113.

[8] R. Cariou, J. Benick, F. Feldmann, et al., Nat Energy 3, 326–333 (2018).

[9] T. Kimoto and J. A. Cooper, Fundamentals of Silicon Carbide Technology: Growth, Characterization, Devices, and Applications, 1st ed. (Wiley, 2014).

[10] S. Asada, T. Kimoto, and J. Suda, IEEE Trans. Electron Devices 64, 3016–3018 (2017).

[11] S. Asada, J. Suda, and T. Kimoto, IEEE Trans. Electron Devices 65, 4786–4791 (2018).

[12] G. P. Li, E. Hackbarth, and T.-C. Chen, IEEE Trans. Electron Devices 35, 89–95 (1988).